Thermal stress analysis of disc brake using analytical and numerical methods

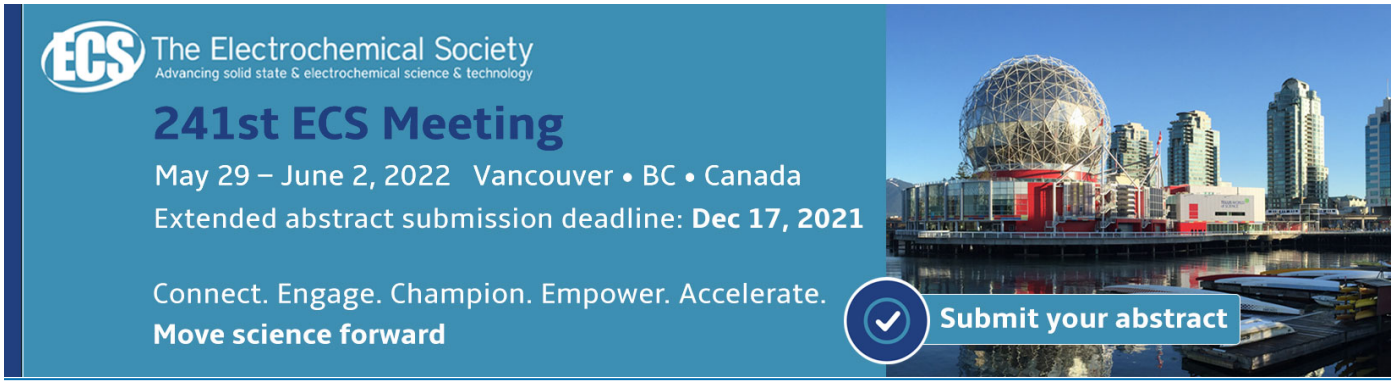

Thermal stress analysis of disc brake using analytical and numerical methods

I T Jiregna[1, *], and H G Lemu[2]

[1] Jimma Institute of Technology, Jimma University, Ethiopia
[2] Faculty of Science and Technology, University of Stavanger, Norway

[*] Corresponding author e-mail: iyasu.jiregna@ju.edu.et

Abstract. This article presents study of the thermal stress development in brake disc and the associated life cycle of the disc. The thermal stress analysis of disc brake under the first brake application and the influences of thermal loads on stress development of the disc have been investigated. The temperature distribution was conducted as a function of disc thickness and braking time. The study was done on the disc brake of Sports Utility Vehicle with a model of DD6470C. Partial solution approach was used to solve analytical temperature distribution through the thickness. The model was done using representative areas of the disc exposed to high temperature whose distribution result was obtained as a function of disc thickness and braking time. The solutions of coupled thermal transient fields and stress fields were obtained based on thermal-structural coupled analysis. Based on the model developed for the study, the positions of high and low stress formations were investigated, and it has been observed that thermal stress and temperature gradient show similar behavior through the thickness of disc. Generally, high temperature and stress components were found on the rubbing surfaces of the disc.

1. Introduction

The amount of accumulated kinetic energy in dynamic mechanical systems is converted into thermal energy at the interface of connecting parts according to the first law of thermodynamics [1]. Vehicle brake system is one type of mechanical system where this conversion process is realized. Therefore, thermal analysis is very important in the study of the brake systems. The disc brake, which is a type of friction brake, is a very critical part of the vehicle and exposed to a nonlinear and thermoelastic loading [2]. It is usually located on the front axle of vehicles and used to adjust or control the speed of vehicle according to the changing road and traffic conditions [3]. A disc brake generates retardation force by converting kinetic energy into thermal energy out of which some amount of heat would be dissipated in the discs by conduction while some other amount is removed to the surrounding by convection or radiation process [4]. The rate of energy conversion from kinetic energy to thermal energy determines the braking power of the system and braking efficiency is determined by the rate of cooling. Thus, if heat dissipation occurs slowly, it will result in the rise of disc temperature and reduce the braking performance and may lead to surface crack propagation.

The work done during the dynamic braking process, which highly influence the generated heat, is a function of, among others, the pressure distribution at the contact interface. While modeling the brake system, two assumptions are mostly applied: (1) constant pressure distribution or (2) constant wear of

the friction material. These assumptions depend on the brake material stiffness where materials with high stiffness are exposed to constant wear across the contact surface [5, 6].

Dynamic braking is usually characterized by nonuniform pressure distribution with time and frictional interface is subjected to not only wear and tear, but also to mechanical and thermal distortion [7]. As a result of this complex loading condition, numerical analysis-based study of the thermal stress distribution of brake systems is widely recommended [8]. For instance, Sen and Sayer [9] conducted study of the elasto-plastic thermal stress of disc brake of steel fiber reinforced composite material using finite element method (FEM) under uniform temperature distribution. The target of the study was to explore the stress components in the radial and tangential directions of the disc. 3D thermomechanical coupling model of a ventilated disc brake was also developed in [3] and the temperature and stress distribution were studied using FEM approach in ANSYS environment.

The objective of this study is to conduct the thermal analysis of the disc brake of a locally selected Sports Utility Vehicle through the investigation of the temperature distribution as a function of disc thickness and braking time. The study employs both analytical and numerical approach and the obtained results are compared. Furthermore, the positions of high and low stress formations are investigated.

2. Materials and methods

2.1. Backgrounds on analysis model

Brake discs can be categorized into two as (1) ventilated brake disc and (2) solid brake disc. In ventilated type of brake disc, air passes through vanes or pillars or between both annular discs, while the solid one consists of a single solid disc. Both types of discs may or may not have a mounting bell which increases the gap between rubbing surface and axle to improve cooling [4] and to protect overheating of wheel bearing. The friction ring (Figure 1) can be fixed on a mounting bell through different methods based on types of disc material. The patents in [10] and [11], as illustrated in Figure 1, state two methods of joining mounting bell with the friction ring. As shown, Figure 1(a) illustrates the joining method through a bolt which is screwed in mounting bell and free to slide along the radial direction in friction ring. This special kind of bolt is made of steel which experiences corrosion and transfers heat to the mounting bell quickly. The tooth in this case would be embedded into the holes prepared on the outer periphery of mounting bell [12]. Figure 1 (b), on the other hand, shows that the connecting ceramic material is used, which can resist corrosion and reduce heat movement from friction ring to the mounting bell.

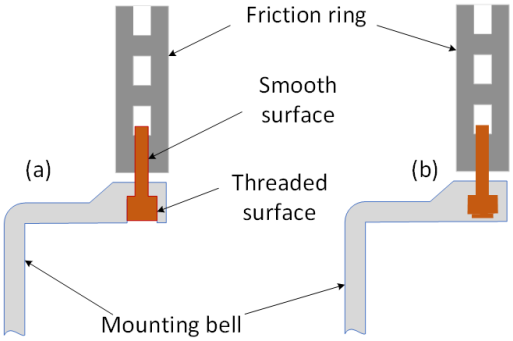

Figure 1. Simplified representation of joining of friction ring and mounting bell with connecting elements using (a) a threaded bolt and (b) a ceramic pin.

2.2. Disc materials

Gray cast iron is a widely used friction material in brakes due to its unique combinations of properties such as very good thermal conductivity, vibration damping ability, high compressive strength and good machinability [13]. In addition, the free graphite in its structure acts as a lubricant which makes it very suitable sliding actions. The stress-strain properties of gray cast iron is also influenced by its composition, i.e. graphite flakes and metal matrix [14]. In addition, the content of graphite provides

important properties [15] such as: dimension stability under different heating condition and high vibration damping. The properties of the brake materials are given in Table 1.

Table 1. Data for gray cast iron with high carbon content.

Number	Material properties	Unit	Pad	Disc
1	Thermal conductivity	$W/m.K$	5	57
2	Density	kg/m^3	1400	7250
3	Specific heat capacity	$J/kg.K$	1000	460
4	Poisson's ratio		0.25	0.28
5	Thermal expansion		10	10.85
6	Young's modulus	GPa	1	138
7	Friction coefficient		0.35	0.35

2.3. Braking condition and assumptions

For the brake model developed in this study, the following conditions were assumed:

1. An average of stopping distance of $81\ m$ at deceleration rate of $8\ m/s^2$ in 4.5 seconds.
2. Ambient temperature of $T_\infty = 30\ ^0C$.
3. Traveling speed of $130\ km/hr$ or $36\ m/s$.
4. Angular speed of disk $300\ rad/s$

In order to simplify the complexities of analysis, the following assumptions were considered.

1. Material properties were assumed to be independent of the temperature and isotropic.
2. Disc and pad nominal contact surface is equal to an apparent surface in sliding motion.
3. Uniformly distributed contact pressure over the friction surfaces, and hence symmetric heat generation of the mid-plane.
4. Due to short brake time, radiation is neglected and hence relatively low temperature.
5. Negligible wear on the contact surface.
6. The heat flux is constant radially and the temperature varies only along thickness.

3. Analytical analysis

3.1. Boundary condition analysis

The analytical model was developed based on the three-fundamental aspect of solid mechanics, namely (1) equilibrium equation, (2) compatibility condition and (3) Hooke's law. The equilibrium equation can be obtained using direct vector or matrix notation [16] given in equation (1) – (3).

$$\frac{\partial \sigma_r}{\partial r} + \frac{1}{r}\frac{\partial \tau_{\theta r}}{\partial \theta} + \frac{\partial \tau_{rz}}{\partial z} + \frac{\sigma_r \sigma_\theta}{r} + F_r = 0 \quad (1)$$

$$\frac{1}{r}\frac{\partial \theta_\theta}{\partial \theta} + \frac{\partial \tau_{r\theta}}{\partial r} + \frac{\partial \tau_{\theta z}}{\partial z} + \frac{\partial \tau_{r\theta}}{r} + F_\theta = 0 \quad (2)$$

$$\frac{\partial \tau_{rz}}{\partial r} + \frac{1}{r}\frac{\partial \tau_{\theta z}}{\partial \theta} + \frac{\partial \sigma_z}{\partial z} + \frac{1}{r}\tau_{rz} + F_z = 0 \quad (3)$$

Where F = external load, σ = normal stress, τ = shearing stress and the subscripts r, z and θ show the directions of radial, circumferential, and axial components respectively.

The compatibility condition is important to satisfy the requirement that distribution of strain and geometry of deformation must be consistent to preserve body continuity [17]. The exact solutions must also satisfy the compatibility requirements. Furthermore, there must be a conformity between loading condition imposed at the boundaries and the stress, strain, and displacement fields.

$$\left(\frac{\partial^2}{\partial r^2}+\frac{1}{r}\frac{\partial}{\partial r}+\frac{1}{r^2}\frac{\partial^2}{\partial \theta^2}+\frac{\partial^2}{\partial z^2}\right)(\sigma_r+\sigma_\theta+\sigma_z+\alpha ET)=0 \quad (4)$$

Where $E =$ Young's modulus, $\alpha =$ coefficient of the linear thermal expansion.

The third aspect of solid mechanics is the Hooke's law (stress strain relations), which states that the material constitutive relations must comply with known behavior of the involved materials. The homogeneous isotropic body in cylindrical coordinate system can be expressed by Hooke's law as [18].

$$\varepsilon_{rr}=\frac{1}{E}[\sigma_{rr}-v(\sigma_{\theta\theta}+\sigma_{zz})]+\alpha\Delta T=\frac{1}{2G}\left(\sigma_{rr}-\frac{v}{1+v}\Theta\right)+\alpha\Delta T \quad (5)$$

$$\varepsilon_{\theta\theta}=\frac{1}{E}[\sigma_{\theta\theta}-v(\sigma_{rr}+\sigma_{zz})]+\alpha\Delta T=\frac{1}{2G}\left(\sigma_{\theta\theta}-\frac{v}{1+v}\Theta\right)+\alpha\Delta T \quad (6)$$

$$\varepsilon_{zz}=\frac{1}{E}[\sigma_{zz}-v(\sigma_{rr}+\sigma_{zz})]+\alpha\Delta T=\frac{1}{2G}\left(\sigma_{zz}-\frac{v}{1+v}\Theta\right)+\alpha\Delta T \quad (7)$$

$$\Theta=\sigma_{rr}+\sigma_{\theta\theta}+\sigma_{zz} \quad (8)$$

Where $E =$ Young's modulus, $\alpha =$ coefficient of the linear thermal expansion, $v =$ Poisson's ratio. $G =$ E/2(1+ v) is the shear modulus and $\Delta T = T(z,t) - T_0$ is the change in temperature.

3.2. Coefficient of heat partition

The partitioning of heat is a function of the thermal properties of the bodies, the contact geometry and the sliding speed [19]. Thermal diffusivity of the pad (ξ_p) and the thermal diffusivity of the disc (ξ_d) were calculated by making use of the values in ***Table 1***.

$$\xi_d=\sqrt{k_d\rho_d c_d}=\sqrt{57*7250*460}=13\,787.50 \quad (9)$$

$$\xi_p=\sqrt{k_p\rho_p c_p}=\sqrt{5*1400*1000}=2\,645.75 \quad (10)$$

The frictional contact surfaces of the pad and the disc S_p and S_d were calculated as follows:

$$S_p=\varphi_0\int_{r_2}^{r_3} rdr=\frac{\varphi}{2}\left(R_p^2-r_p^2\right)=\frac{65^0}{2}(0.12^2-0.06^2)=0.006\ m^2 \quad (11)$$

$$S_d=2\pi\int_{r_2}^{r_3} rdr=\pi(R_d^2-r_d^2)\pi(0.12^2-0.06^2)=0.034\ m^2 \quad (12)$$

The contact surface elements on which the integration is valid is illustrated in Figure 2.

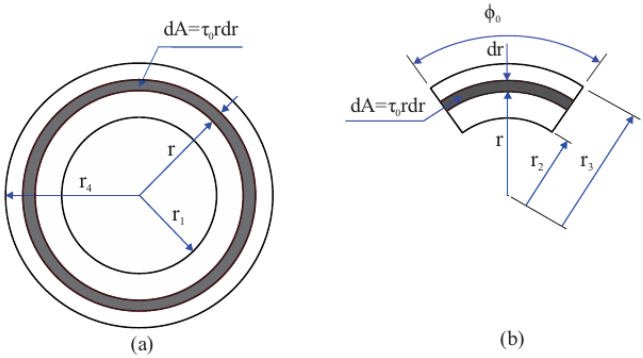

Figure 2. Contact surface elements of (a) the disc and (b) the pad.

On the rubbing interface of the disc and the pads, the total heat generated q equals summation of heat flux into the disk q_d, and heat flux into the pad q_p. Then, the coefficient of partition γ was obtained by using equation (13).

$$\gamma = \frac{\xi_d S_d}{\xi_d S_d + \xi_p S_p} = \frac{13\,787.50 * 0.034}{13\,787.50 * 0.034 + 2\,645.75 * 0.006} = 0.96 \tag{13}$$

3.3. Heat flux inputs to the disc and pads

The heat flux at the surfaces is obtained from the ratio of the thermal energy and the surface contact area of each component. The rate of heat generated due to friction between these surfaces is calculated as [20].

$$d\dot{E} = dp = r\omega\mu p\varphi_0 r dr \tag{14}$$

$$d\dot{E} = d\dot{E}_p + d\dot{E}_d \tag{15}$$

$$d\dot{E}_p = (1-\gamma)dp = (1-\gamma)\omega\mu p\varphi_0 r^2 dr \tag{16}$$

$$d\dot{E}_d = \gamma dp = \gamma\omega\mu p\varphi_0 r^2 dr \tag{17}$$

Where $d\dot{E} =$ the heat generation rate due to friction between sliding parts, $V =$ the relative sliding velocity, $dF_f =$ the friction force, $dE_p =$ the absorbed heat by the pad and dE_d is the amount of absorbed heat by the disc.

The pressure distribution has categories of uniform pressure and uniform wear pressure distribution. In the case of uniform pressure $P = P_{max}$ and heat flux is a function of time and space variable r. Because, during braking, angular velocity will decrease with time and the increase in radial space variable will result in growth of work done by friction force. The heat flux q on a contact area is updated per the pressure distribution and the heat flux in the pad can be given by the following equations.

$$q_p(r,t) = \frac{d\dot{E}_p}{dS_p} = \frac{(1-\gamma)\omega\mu p\varphi_0 r^2 dr}{\varphi_0 r dr} = (1-\gamma)\mu pr\omega(t) \tag{18}$$

$$q_{0p}(r) = q_{01}(r,0)\frac{d\dot{E}_p}{dS_p} = \frac{(1-\gamma)\omega\mu p\varphi_0 r^2 dr}{\varphi_0 r dr}(1-\gamma)\mu pr\omega_0 \tag{19}$$

Moreover, for disc or rotor, the heat flux could be expressed as:

$$q_d(r,t) = \frac{d\dot{E}_d}{dS_d} = \frac{\gamma\omega\mu p\varphi_0 r^2 dr}{2\pi r dr} = \frac{\varphi_0}{2\pi}\gamma\mu pr\omega(t) \tag{20}$$

$$q_{0d}(\mathrm{r}) = \frac{d\dot{E}_d}{dS_d} = \frac{\gamma\omega\mu p\varphi_0 r^2 dr}{2\pi r dr} = \frac{\varphi_0}{2\pi}\gamma\mu pr\omega_0 \tag{21}$$

Where $dS_d =$ Surface contact area of disc and $dS_p =$ Surface contact area of pads.

The uniform wear pressure approach is more realistic after several braking application and the heat flux in this case is a function of time and it is independent of the space variable, i.e., the work done by friction force is the same at radial direction. Then by inserting $p = p_{max}\,{}^{r_p}/_{r}$ into equations (18) and (20), the following expressions could be obtained respectively.

$$q_p(r,t) = (1-\gamma)\mu p_{max} r_p \omega_0 \left(1 - \frac{t}{t_b}\right) \tag{22}$$

$$q_d(r,t) = q_{0d}(r) * \left(1 - \frac{t}{t_b}\right) \tag{23}$$

$$q_d(r,t) = \frac{\varphi_0}{2\pi}\gamma\mu p_{max} r_d \omega_0 * \left(1 - \frac{t}{t_b}\right) \tag{24}$$

3.4. Disc thermal stress analysis

The stress σ_z suppress thermal expansion of the disc along circumferential and σ_θ suppress expansion along axial direction. Furthermore, taking $\varepsilon_z = 0$, $\sigma_z = 0$ and $\varepsilon_\theta = 0$, the following equation is stated [21].

$$\sigma_{zz} = \sigma_{\theta\theta} = -\frac{\alpha E \Delta T}{1-v} \tag{25}$$

The transient stress, on the other hand, is expressed as a function of thickness of the disc.

$$\sigma_{zz} = \sigma_{\theta\theta} = -\frac{\alpha E}{1-v}\frac{q_0\delta}{k}\left[-\frac{1}{6}+\frac{\alpha}{\delta^2}t+\frac{z^2}{2\delta^2}-2\sum_{n=1}\frac{(-1)^n}{\lambda_n^2}\cos\left(\lambda_n\frac{z}{\delta}\right)e^{-\lambda_n^2\left(\frac{\alpha}{\delta^2}\right)t}\right] \tag{26}$$

This equation is valid if and only if thermal variation follows the direction perpendicular to Z and along θ direction. To obtain the axial stress, the difference between the outer surface temperature T_1 and inner surface temperature T_2 is used. Therefore, equation (26) is modified as:

$$\sigma_{zz} = -\frac{\alpha E}{1-v}\left(T_1(t) - T_2(t)\right) \tag{27}$$

Due to the equal and opposite tensile force of intensity $\alpha E T$ on the edges, the stress in disc is superposed on equation (26) to give thermal stress free from external force. The resultant force is:

$$F_R = \int_0^\delta \alpha E \Delta T dz \tag{28}$$

Whereas, a uniformly distributed radial tensile stress formed in disc can be expressed by:

$$\frac{1}{\delta(1-v)}\int_0^\delta \alpha E \Delta T dz \tag{29}$$

Then, by inserting equation (28) into compressive radial stress, the radial thermal stress is obtained as:

$$\begin{aligned}\sigma_{rr} = &-\frac{\alpha E}{1-v}\frac{q_0\delta}{k}\left[-\frac{1}{6}+\frac{\alpha}{\delta^2}t+\frac{z^2}{2\delta^2}-2\sum_{n=1}\frac{(-1)^n}{\lambda_n^2}\cos\left(\lambda_n\frac{z}{\delta}\right)e^{-\lambda_n^2\left(\frac{\alpha}{\delta^2}\right)t}\right] \\ &+\frac{\alpha E q_0\delta}{k\delta(1-v)}\int_0^\delta\left[-\frac{1}{6}+\frac{\alpha}{\delta^2}t+\frac{z^2}{2\delta^2}-2\sum_{n=1}\frac{(-1)^n}{\lambda_n^2}\cos\left(\lambda_n\frac{z}{\delta}\right)e^{-\lambda_n^2\left(\frac{\alpha}{\delta^2}\right)t}\right]dz\end{aligned} \tag{30}$$

Where T is considered as a function of z with a mean value of zero over disc thickness. But if the mean value of T is different from zero, the tensions along r and z directions corresponding to the edge resultant force could be superposed on equation (25). Furthermore, along rz plane temperature is not symmetric which leads to add bending stress on the equation. Distribution of shear stress do not exist as a result of boundary condition symmetry. Therefore, for known value of temperature distribution T over disc thickness, thermal stress is obtained using equation (31).

$$\sigma_{rr} = \frac{\alpha E \Delta T}{1-v} + \frac{1}{\delta(1-v)}\int_0^\delta \alpha E \Delta T dz + \frac{24z}{2\delta^3(1-v)}\int_0^\delta \alpha E T dz \tag{31}$$

3.5. von-Mises analysis

The thermal stress developed by distribution of temperature is evaluated by elastic von-Mises stress σ_e defined in equation (32), which relates the three principal stresses and determines the yield (plastic deformation onset) in metals.

$$\sigma_e = \frac{1}{\sqrt{2}}\left[(\sigma_r-\sigma_\theta)^2+(\sigma_\theta-\sigma_z)^2+(\sigma_z-\sigma_r)^2\right]^{1/2} \tag{32}$$

4. FEM Analysis

4.1. FEM temperature distribution analysis

The FEM study on temperature distribution shows that maximum temperature obtained is 139.3 ℃ while the minimum temperature of 78.08 ℃ is located on the other surface far from the rubbing surface. This variation in the values of temperature shows that the thermal gradient occurs along the thickness of the disc as shown in Figure 3.

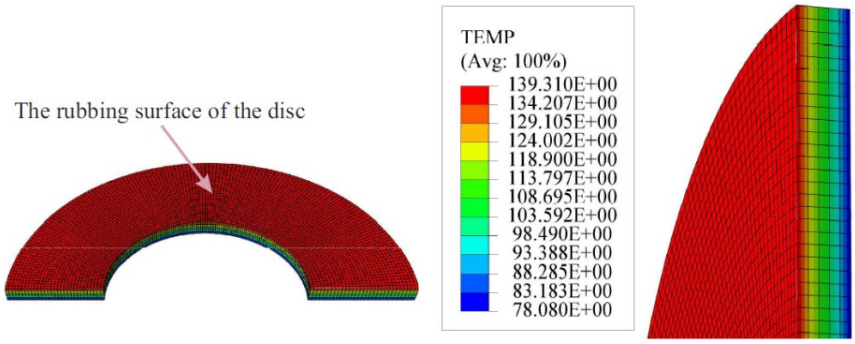

Figure 3. Temperature distribution through the thickness of the disc.

4.2. FEM Circumferential Stress Analysis

At the rubbing surface, high circumferential stress is obtained and this value of stress drops as the thickness moves away from the friction surface. The maximum compressive circumferential stress is found on the rubbing surface of the disc and its value is 276 MPa. Whereas, the minimum compressive circumferential stress is obtained on the surface far from rubbing surface with the value of 122 MPa (Figure 4).

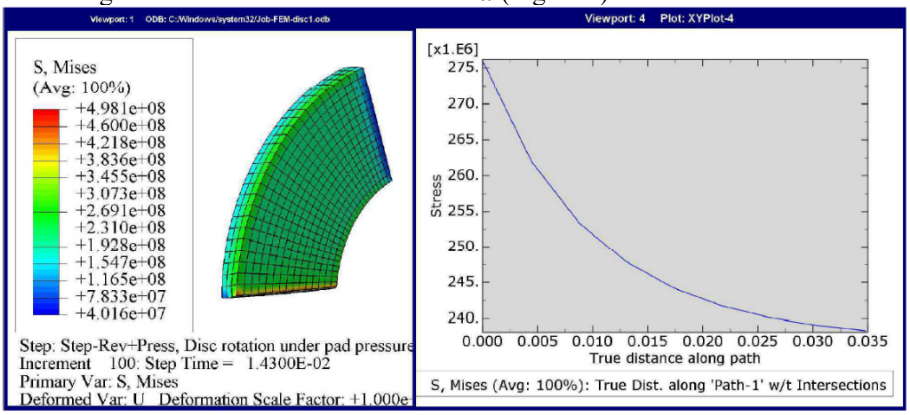

Figure 4. Circumferential stress through the thickness of the disc.

4.3. FEM radial stress analysis

The outer portion of the disc thickness is subjected to tensile radial stress and the other portion far from rubbing surface is subjected to compressive radial stresses. The maximum tensile radial stress is observed on the rubbing surface is 58.8 MPa. The value of tensile radial stress decreases as the thickness increases from the rubbing surface and beyond half of the thickness of the disc, a compressive stress rises up to the end of the thickness as shown in Figure 5.

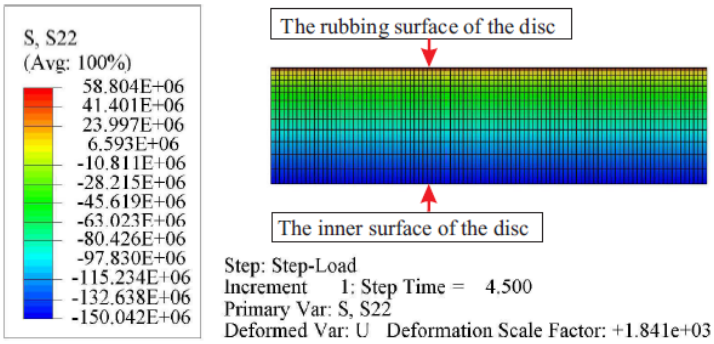

Figure 5. Radial stress through the thickness of the disc.

4.4. FEM von-Mises stress analysis

As shown in contour plot of Figure 6, the maximum and minimum von-Mises stresses are observed on the sharp edges with the maximum of 498.3 MPa and the minimum of 73.9 MPa. The surface far from rubbing surface is subjected to high thermal stresses than the rubbing face because it is constrained from any thermal expansion due to symmetry and therefore, resists radial expansion.

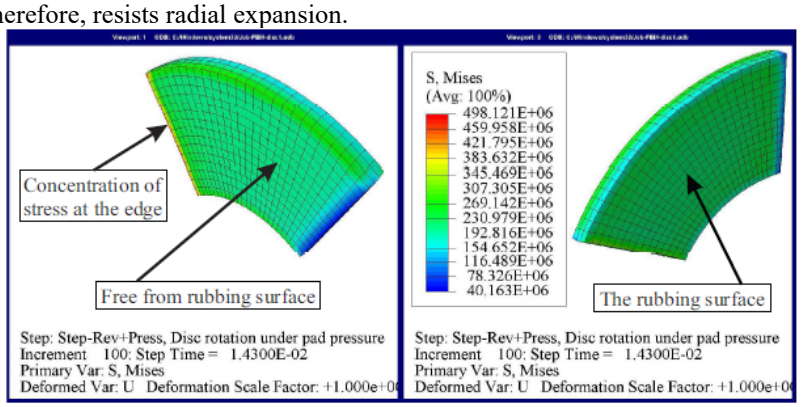

Figure 6. von-Mises stress distribution through the thickness of the disc.

5. Discussion

5.1. Temperature distribution in the disc

The steady-state temperature difference of the friction surface and lower part of the disc shown in Figure 7(a) is 61.22 ℃ by FEM analysis and 65.65 ℃ by analytical analysis after simulation over 4.5 seconds. The transient temperature distribution through braking time is shown in Figure 7(b). The temperature distribution in both cases shows good agreement between the analytical and numerical methods.

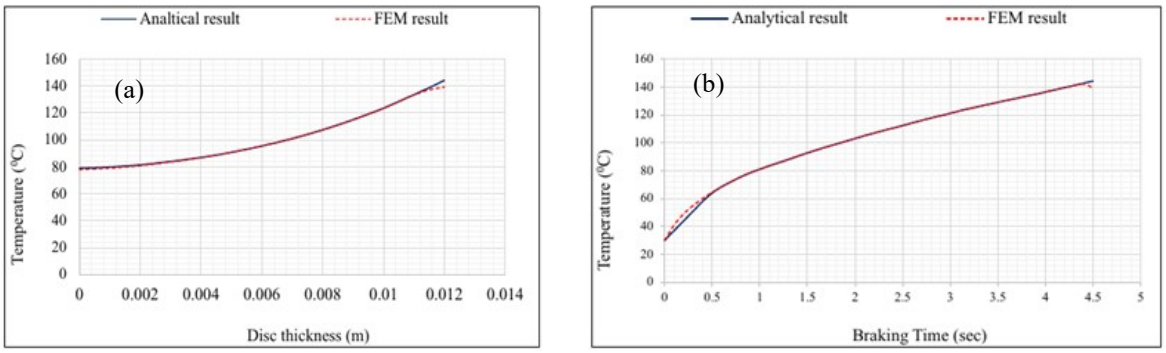

Figure 7. (a) Steady state temperature distribution and (b) Transient surface temperature distributions.

5.2. Circumferential and radial stress distributions along disc thickness

The minimum circumferential stress is obtained to be $-122\ MPa$ based on FEM analysis and $-165\ MPa$ based on analytical analysis. This minimum stress is located far from the rubbing surface where minimum temperature is located. The maximum circumferential compressive stress by FEM analysis is found to be $-276\ MPa$, and by analytical analysis is $-388\ MPa$ as shown in Figure 8(a). In this analysis, the analytical approach overestimated the compressive stress throughout the thickness.

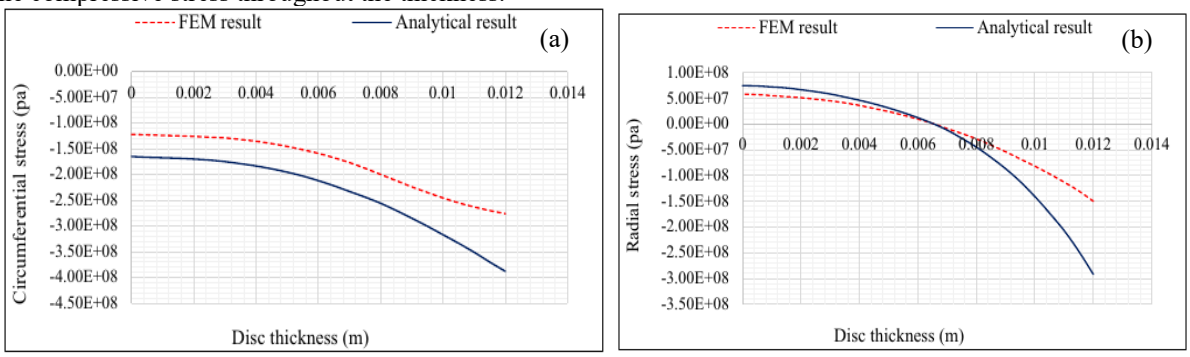

Figure 8. (a) Compressive circumferential stresses and (b) Radial stresses as a function of disc thickness.

As illustrated in Figure 8(b), the radial stresses are tensile from $0\ mm$ to $6.6\ mm$ thickness of disc and compressive stresses occur in the other portion of thickness. The maximum tensile stress at the lower surface of the disc is $58.8\ MPa$ by FEM and the analytical result obtained was $74.2\ MPa$.

5.3. Axial stress and von-Mises stress distribution along disc thickness

Figure 9 shows the stress distribution in axial direction and the von Mises equivalent stresses evaluated analytically and FEM approach. The direction of temperature distribution in the disc is parallel to an axial stress so it does not interrupt the axial stress through the thickness of the disc. The axial stress obtained analytically is $-220\ MPa$ and it is constant throughout the thickness of the disc whereas the value obtained by FEM is $-175\ MPa$ with negligible variation throughout disc thickness (Figure 9(a)).

As the plots in Figure 9(b) illustrate, the analytical solutions have similar trend of von Mises stress variation though the thickness as the FEM results. The highest von Mises stress results obtained by analytical method is $269\ MPa$ while the FEM was $215\ MPa$. These results were obtained at the inner surface of the disc and this is because the pressure distribution is inverse function of the radius. The surface area where the maximum von Mises stress obtained is far from the edges formed from sectional representation of the model due to symmetric conditions of the disc. Due to possible high stress concentration on the sharp edges, the result was taken from the middle of the surface of the disc.

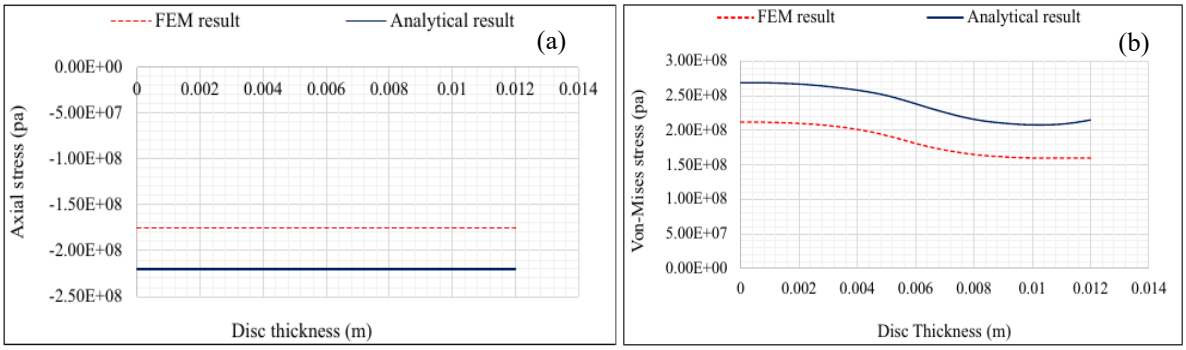

Figure 9. (a) Axial stress through the thickness of the disc (b) von-Mises stress through thickness.

6. Conclusions

In this study, both analytical and FEM based approaches have been employed to study the thermal stress development through the thickness of the brake disc under a single brake application. The methods of analysis followed in this study are thought to be a good approach to investigate the stresses in sliding mechanical components. The fact that the results obtained from both analytical and FEM methods are close to each other is that the procedures followed have addressed the analysis correctly.

In thermal analysis, the temperature distribution was conducted as a function of disc thickness and braking time and the results obtained in both analytical and FEM are similar. Furthermore, the positions of high and low stress formations are investigated, and thermal stress and temperature gradient show similar behavior through the thickness of the disc. From the obtained analysis results, the axial stress was constant throughout disc thickness with a result of $-220\ MPa$ analytically while the result obtained by FEM is $-175\ MPa$. The circumferential stress variation through disc thickness, on the other hand, is high which is $-388\ MPa$ at rubbing surface and $-165\ MPa$ at the surface far from rubbing surface by analytical analysis approach. In contrast, the FEM approach gave $-276\ MPa$ at rubbing surface and $-122\ MPa$ at the surface far from rubbing surface. Whereas, in radial stress analysis, compressive stress was observed on the rubbing surface of the disc and tensile stress occurs on the surface far from rubbing surfaces with a result of $74.2\ MPa$ analytically and $58.8\ MPa$ by FEM.

In contour plot of von-Mises stresses, it could not show the correct result of the stress through the thickness of the disc because the sharp edges of the disc are exposed to stress concentration leading to variation of the von Mises results at the edges and those the surfaces far from the edges. Thus, the von-Mises stress values around the middle from both sectioned edges is taken using path cross section through the disc thickness to represent the whole disc and the result obtained through this method is $215\ MPa$ which is very close to the result of the analytical approach of $269\ MPa$.

Generally, high temperature and stress components were found on the rubbing surfaces of the disc, which result in fast surface crack propagation. Because the cyclic compressive and tensile stresses due to temperature variation drive the crack by changing the crack tip properties.

References

[1] Ashtekar A 2000 Interface of general relativity, quantum physics and statistical mechanics: Some recent developments, *Ann. Phys.* **9**(3–5), 178–198.
[2] Afzal A, Abdul Mujeebu M 2019 Thermo-mechanical and structural performances of automobile disc brakes: A review of numerical and experimental studies, *Arch. Comput. Methods Eng.* **26**, 1489–1513.
[3] Belhocine A, Bouchetara M 2013 Investigation of temperature and thermal stress in ventilated disc brake based on 3D thermomechanical coupling model. *Ain Shams Eng. J.* **4**(3), 475 – 483.
[4] Kinkaid N, O'Reilly O M and Papadopoulos P 2003 Automotive disc brake squeal, *J. Sound Vib.* 267(1), 105 – 166.
[5] Ghadimi B, Kowsary F and Khorami M 2013 Thermal analysis of locomotive wheel-mounted brake disc, Appl. *Therm. Eng.* **51**(1–2), 948–952.
[6] Khairnar H P, Phalle V M and Mantha S S 2016 Comparative frictional analysis of automobile drum and disc brakes, *Tribol. Ind.* **38**(1), 11–23.
[7] Chen F 2009 Automotive disk brake squeal: an overview, *Int. J. Veh. Des.* **51**(1–2), 39–72.
[8] Söderberg A and Andersson S 2009 Simulation of wear and contact pressure distribution at the pad-to-rotor interface in a disc brake using general purpose finite element analysis software. *Wear* **267**(12), 2243–2251.
[9] Sen F and Sayer M 2006 Elasto-plastic thermal stress analysis in a thermoplastic composite disc under uniform temperature using FEM, *Math. Comput. Appl.* **11**, 31-39.
[10] Holger Keller Inventions, Patents and Patent Applications - Justia Patents Search [Internet]. [cited 2021 Jun 14]. Available from: https://patents.justia.com/inventor/holger-keller.
[11] Struve J, Franke M. Automatic Locking of a Wind Turbine [Internet]. 2005 [cited 2021 Jun 14]. Available from: https://patentscope.wipo.int/search/en/detail.jsf?docId=WO2005090780.
[12] Disc Brakes Patents and Patent Applications (Class 188/18A) - Justia Patents Search [Internet]. [cited 2021 Jun 14]. Available from: https://patents.justia.com/patents-by-us-classification/188/18A.
[13] Diószegi A, Fourlakidis V and Svensson I L 2004. Microstructure and tensile properties of grey cast iron.

Research Report, Jönköning Univedrsity, Sweden.
[14] Cho M H, Kim S J, Basch R H, Fash J W and Jang H 2003 Tribological study of gray cast iron with automotive brake linings: The effect of rotor microstructure. *Tribol Int.* **36**(7), 537–545.
[15] Moghadam A D, Omrani E, Menezes P L and Rohatgi P K 2015 Mechanical and tribological properties of self-lubricating metal matrix nanocomposites reinforced by carbon nanotubes (CNTs) and graphene–a review, *Compos. Part B Eng*. **77,** 402–420.
[16] Kane J H 1994 *Boundary element analysis in engineering continuum mechanics*. Englewood Cliffs NJ Prentice Hall 1994.
[17] Kundu T 2012 *Fundamentals of fracture mechanics*. CRC Press, Taylor & Francis Group London UK.
[18] Evtushenko O O, Ivanyk E H and Horbachova N V 2000 Analytic methods for thermal calculation of brakes. *Mater Sci.* **36**(6), 857–862.
[19] Rashid A 2013 Simulation of thermal stresses in a brake disc, *PhD Thesis*. Linköping University Electronic Press, Sweden.
[20] Talati F and Jalalifar S 2009 Analysis of heat conduction in a disk brake system. *Heat Mass Transf.* **45**(8), 1047.
[21] Timoshenko S P and Goodier J N 1970, *Theory of Elasticity*. McGraw-Hill, New York, USA.